Faradjizadeh, F.; Vilathgamuwa, M.; Jovanovic, D.; Jayathurathnage, Prasad; Ledwich, G.; Madawala, U.

Expandable N-Legged Converter to Drive Closely Spaced Multi Transmitter Wireless Power Transfer Systems for Dynamic Charging

Published in:
IEEE Transactions on Power Electronics

DOI:
10.1109/TPEL.2019.2939848

Published: 01/04/2020

Document Version
Peer-reviewed accepted author manuscript, also known as Final accepted manuscript or Post-print

Please cite the original version:
Faradjizadeh, F., Vilathgamuwa, M., Jovanovic, D., Jayathurathnage, P., Ledwich, G., & Madawala, U. (2020). Expandable N-Legged Converter to Drive Closely Spaced Multi Transmitter Wireless Power Transfer Systems for Dynamic Charging. *IEEE Transactions on Power Electronics*, *35*(4), 3794-3806. Article 8827310. https://doi.org/10.1109/TPEL.2019.2939848

Expandable N-Legged Converter to Drive Closely Spaced Multi Transmitter Wireless Power Transfer Systems for Dynamic Charging

F. Farajizadeh, *Student member, IEEE*, M. Vilathgamuwa, *Senior Member, IEEE,* D. Jovanovic, *Member, IEEE,* P. Jayathurathnage, *Member, IEEE*, G. Ledwich, *Senior Member, IEEE*, U. Madawala, *Fellow,*

ABSTRACT

Expandable and flexible wireless power transfer (WPT) systems have been in demand in numerous industry applications, especially for dynamic chargers in electric vehicles. Those systems, however, brings about certain technical issues such as modulation technique and topology of the transmitter-side, and transferred power profile of the transmitters. In this paper, a new converter topology to drive closely spaced segmented Dynamic Wireless Power Transfer (DWPT) systems is proposed. The proposed converter can be expanded to cater for different number of transmitters, and it can provide a uniform transferred power profile throughout the path of transmitter coils, known as track. Furthermore, this study focuses on analyzing the operation of the converter and the effect of closely spaced transmitters over its operation. To show the effectiveness of the proposed topology and its modulation technique, the converter is simulated and experimentally tested using a laboratory prototype. The results are compared and analyzed, and their close agreement shows the validity of the proposed technique.

Index Terms—Cross Coupling, Coordination Factor, Electric Vehicles, Expandable Wireless Power Transfer System, Inductive Charging, Magnetic Profile, Mode Changing Transients, Multi-Transmitter Wireless Power Transfer Systems, Transferred Power Profile.

I. INTRODUCTION

Amongst all carbon emitting contributors, fossil fuel vehicles have a significant influence on air pollution. The use of either Electric Vehicles (EVs) is one of the most effective solutions to address this issue [1, 2]. EVs still find it difficult competing against their fossil fuel counterparts, especially in terms of power and energy density [1]. The placement of higher number of accessible electric chargers along the way can be seen as a sensible approach [3]. However, wired chargers are stationary and the vehicles must stop at the charging station to get charged [4], the mechanical connectors need to be serviced regularly [5], and they are not completely safe in wet or dirty environments [6]. As an alternative, wireless charging can solve these issues. Wireless charging process can be done either stationary, while the EV is stopped, or dynamically, while it is on the move [7]. However, the use of dynamic chargers is more advantageous as they save the driver's time. Furthermore, Dynamic Wireless Power Transfer (DWPT) increases the driver's safety, enhances the reliability of the system and decreases the maintenance costs, as it does not need any mechanical connectors for charging [8].

Transmitters in DWPT systems can be divided into two main categories of elongated transmitters and segmented transmitters [9]. In the elongated type, a long coil acts as the transmitter which is laid along the track. However, in this method, the magnetic flux produced by the transmitter is not confined, and the ratio between linkage and leakage fluxes is significantly small. This leads to high electromagnetic interferences and a high level of electromagnetic exposure from the non-interactive parts of the transmitter. In terms of electric concerns, power losses in the non-interactive part of the transmitter and the size of compensators and power supplies to drive the transmitter are the main drawbacks of the elongated transmitter [4, 10-15]. Moreover, the reliability of the system is dependent on the length of the transmitter, and in case of any failure, all the length of coverage would malfunction.

In the other method of DWPT, i.e. in segmented transmitters, several transmitters are deployed in a track, and they can be driven by one or more than one converter [10]. This method addresses the issues of undesirable losses and exposure in non-interactive parts [4, 11, 16], electromagnetic interferences [4, 12], and high ratings of drivers and compensators [12, 14]. However, making a uniform transferred power profile is not easily achievable, and if transmitters are not closely spaced, the linkage flux would be even less than that of the elongated type [11, 16-18].

To expand and refine the transferred power profile, Budhia et al. in [6] have established the concept of double windings, also known as DD windings, on the track side which are magnetically connected in series and electrically connected in parallel. This approach not only expands the coverage of transmitter magnetic field, but also removes the power null between DD transmitters. To remove the power null, in addition to DD windings, another quadrature winding, known as Q winding, is also used on the pickup side.

To develop the DDQ concept into an expandable pattern, [12] and [19] use adjacent multiple DD transmitters and drive them in parallel through a H-Bridge converter. While this approach is successful in expanding the transferred power profile along the pickup direction, currents in all transmitters are almost equal and cannot be controlled individually, and that results in undesirable power losses in non-interactive transmitters. The lack of controllability in transmitter currents can also lead to power profile fluctuations, which make power tracking difficult in the pickup side.

In [20], a comprehensive study over magnetic profiles of different types of DDQ topologies, especially when coils are driven independently, is carried out. However, the effect of cross coupling amongst the adjacent transmitters on the driving converters is not studied. To tackle this problem, [2] uses individually driven DD coils with a specific arrangements to make a uniform transferred power profile. In this method, however, the cross coupling between transmitters prevents the close positioning of the transmitters, and consequent spacing of transmitters cannot effectively contribute to alleviate the bumps of transferred power. In all of these DD(/Q) based methods, although the smart approach of using Q winding improves the power profile of the system, excessive use of wires and ferrites, and the lack of controllability in each transmitter (each of D or Q windings) are two weak points of this approach.

In [21], a multi-leg inverter is proposed to provide a more economical arrangement to drive dynamic wireless systems for EV applications. However, enhancement of transferred power profile, soft switching, and mode changing transients has not been studied, as the main concern of the paper was load detection.

Therefore, taking the advantage of a refined LCC compensator introduced in [22], an expandable N-Legged Converter (NLC) is proposed to drive a closely spaced segmented DWPT system, as shown in Fig. 1. The resultant system is capable of making a uniform power profile for the pickup at a high efficiency. This can be achieved with a reduced number of power electronic switches in the driving system and a less volume of copper and ferrite in the magnetic system compared to the conventional systems. A brief comparison of the proposed converter with the conventional DDQ system is presented in [23]. In this paper, a more in-depth study is done on the effect of cross couplings amongst the transmitters, and transition between different modes of operation. Furthermore, the system is experimentally built and tested.

The proposed converter consists of n legs that can individually drive the coils with a reduced number of switches to form a desirable transferred power profile. Moreover, based on the method proposed in [22], a refined compensator that can mitigate the undesirable effect of cross coupling in the transmitters is used. In the process of achieving a desirable transferred power profile, different modes of operation are defined for NLC and they are changed with the position of the pickup. As shown in Fig. 1, the pickup position must be sensed and sent to the driving system. So far, studies have shown some promising results in the realm of pickup position estimation by directly measuring WPT coil-compensator current and voltages [24-27], or with the use of additional sensing systems [28, 29], and yet some more accurate and fast techniques are being investigated. Position estimation is important particularly in EVs to make them smarter, especially for auto piloting. With the use of some of these sensors and communications link between them and the WPT transmitters deployed on the road, accurate detection of pickup position is not that a far-fetched preposition. However, as the estimation of the pickup position is not the main concern of this paper, a simple infrared sensor is used to detect the position of the pickup and a gradual change of modes with the knowledge of system parameters is adopted to mitigate the mode changing transients. Owing to the presence of multiple legs in the NLC, the converter possesses a remarkable reliability and tolerance against faults, and this aspect is to be comprehensively studied in a subsequent work.

Fig.1 shows a generic view of the proposed system studied in this paper. The expandable converter is presented in section II. The converter drives a closely spaced magnetic system, consisting of $n-1$ transmitters and one receiver (r).

The magnetic system is studied in section III. The transmission of power from the NLC to the transmitters is done through a refined LCC compensators, comprising of an inductor, two capacitors and a coupled inductor, which is explained in detail in section IV. Pickup position is detected by a position detection system comprising of an infrared sensor, a first order filter, a hysteresis controller, a ramp filter, and a PWM signal generator. The mode changing strategy to suppress undesirable transients is proposed in section V.

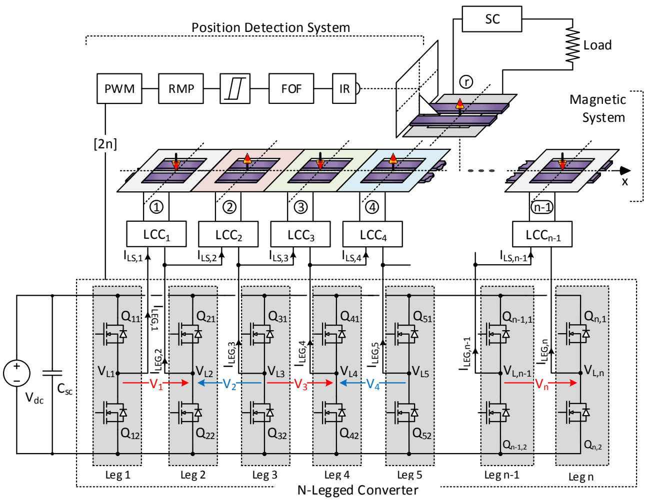

Fig. 1: Generic view of NLC driving a segmented DWPT. In this figure RMP stands for ramp controller, FOF is used for the first order filter, IR stands for infrared sensor, SC is series compensator, and LCC is the type of compensators used in the transmitters.

To validate the mathematical concepts, the system is simulated based on the specifications given in TABLE. 1 by ANSYS Electronics Desktop/Maxwell [30] and MATLAB/Simscape/Fundamental Blocks/Power Electronics [31], and the results are shown in the respective sections. Moreover, experiments are conducted for further validation of the proposed concept, and corresponding experimental results are shown in section VII.

II. Operation of the Converter

To drive a multi-transmitter segmented DWPT system effectively, the maintenance of transferred power quality and efficiency is of prime concern. This can be addressed by closely spacing the transmitters in the system (as explained in section III) and by appropriately exciting the transmitters corresponding to the pickup position. To enhance the efficiency, the transmitters, which are not effectively coupled with the pickup, should be turned off. For this purpose, the flow of power in each transmitter must be controlled. In this section, a new converter with a low number of power electronic switches is presented to serve this purpose.

As shown in Fig. 1, the proposed converter comprises of n number of legs, which are connected in parallel, and they can form $n-1$ pairs of adjacent output terminals. The output terminals can be used to drive an expandable segmented DWPT system. The control parameter to change the output voltage is the difference of voltage phase angles in two adjacent legs, represented as $\Delta D_i = D_{i+1} - D_i$. Therefore, the converter can change its output leg-to-leg voltage of V_i according to (1). Fig. 2 shows the waveforms of leg-to-ground and leg-to-leg voltages of two adjacent legs, and Fig. 3 depicts the voltage phasors of the leg-to-ground and leg-to-leg fundamentals.

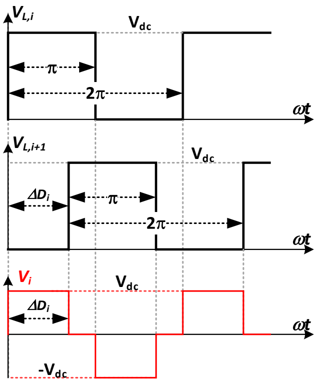

Fig. 2. Leg-to-ground and leg-to-leg voltages of two adjacent legs.

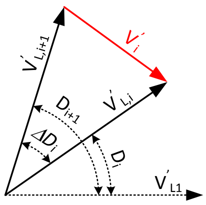

Fig. 3. Voltage phasor diagram of leg-to-ground ($V_{L,i}$) and leg-to-leg (V_i) fundamentals of adjacent legs in an NLC ($V'_{L,i}$ is the fundamental component of $V_{L,i}$).

$$V_i = \underbrace{\frac{2}{\pi} V_{dc} \sin\left(\frac{D_{i+1} - D_i}{2}\right)}_{V_m} \angle \underbrace{\left(\frac{D_{i+1} + D_i}{2} - \frac{\pi}{2}\right)}_{\theta} \tag{1}$$

where V_m and θ are the amplitude and phase angle of V_i respectively.

In segmented DWPT systems, the maximum transferred power occurs when the magnetic fields of all transmitters are in the same phase and the same magnetic polarity. This is similar to the summation of many vectors which will reach the maximum value when all the vectors are aligned and in the same direction [32, 33]. In the proposed converter, the maximum output voltage of two adjacent pair of terminals occurs when their phase angles are 180° out of phase, as shown in Fig. 3. Therefore, to make two identically wound coils produce their maximum magnetic fields along the same direction, the terminals of every other coil must be flipped when they are connected to the NLC output terminals.

As an example, assuming that in the multi-transmitter DWPT system shown in Fig. 1, transmitter i is at its desirable coupling level, by applying $\Delta D_i = D_{i+1} - D_i = 180°$ or $-180°$ to the phase angle between legs i and $i+1$, transmitter i can have the highest voltage, and as a result it can transfer the highest power to the pickup. Meanwhile for other transmitters where the coupling level is low, the phase angle between their corresponding adjacent legs in the NLC should be kept zero to turn off the transmitters such that unnecessary losses are prevented. Similar analogy can be used to explain when two (i and $i+1$) or more (e.g. i, $i+1$, and $i+2$) transmitters have a desirable coupling with the pickup at a time. In those cases, the converter can provide the interacted coils with the maximum voltage and turn off the other ones ($\Delta D_i = 180°$, $\Delta D_{i+1} = -180°$, for two interactive coils, and in case of involvement of the third coil $\Delta D_{i+2} = 180°$).

How to define the modes of operation in a regularly distributed multi-transmitter segmented DWPT, and use NLC to drive the DWPT system is explained in the following sections.

III. Trans Coupling and Magnetic Coordination

As shown in Fig.4, in segmented DWPT systems, there are different types of couplings that take place while the system operates. In terms of transferred power, the desirable couplings are the ones that occur between transmitters and receivers, ($L_{i-1,r}$, $L_{i,r}$ and $L_{i+1,r}$) which from here onwards are defined as trans couplings. Moreover, the undesirable couplings that happen between the coils at either receiver or transmitter side ($L_{i-1,i}$, $L_{i,i+1}$ and $L_{i-1,i+1}$) and are known as cross couplings.

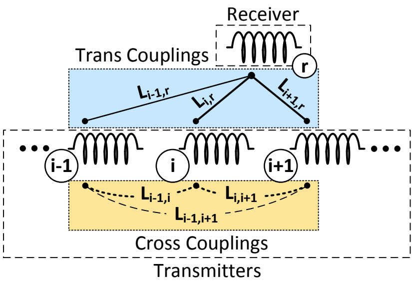

Fig. 4. Couplings in a segmented DWPT system.

One of the main goals of this paper is to form a uniform trans coupling profile in a segmented DWPT system as it can give rise to a uniform transferred power [23]. This is not achievable unless the transmitters are placed near to each other, which will in turn increase the cross coupling between them. The undesirable effect of the cross coupling between transmitter coils is disruption of soft-switching in the driving power converters. This phenomenon creates a shift between voltage and current zero crossing transitions of the NLC switches, causing some residual current at the instant of voltage zero crossing and when switches are turned on or turned off. This is also known as hard switching and will lead to a higher power loss or even thermal failure of the switches. Here, the influence of cross coupling on this current is analyzed and handled using a refined LCC compensator proposed in [22].

As shown in Fig. 4, in a segmented DWPT system with one receiver coil and multiple transmitters, the induced voltage in the coil can be expressed as follows:

$$E_n = s \sum_{i=1}^{n-1} L_{ir} I_i \tag{2}$$

where L_{ir} is the trans coupling between the i^{th} transmitter and the receiver, and I_i is the i^{th} transmitter current. The induced voltage E_n is the main source of energy at the receiver side and acts as a current-controlled voltage source. This voltage is linked to the current of each transmitter through the corresponding trans coupling. Therefore, by properly designing the magnetic system and injecting appropriate current into the transmitters, a continuous profile of voltage is achievable. To have a dedicated criterion for this contribution of trans couplings and injected currents, a coordination factor χ, as given in (3a), can be defined.

$$\chi = L_{1r} I_1 + L_{2r} I_2 + \cdots + L_{n-1,r} I_{n-1} \tag{3a}$$

$$I_r = \frac{\omega \chi}{R_L} \Rightarrow P_{out} = \frac{\omega^2 \chi^2}{R_L} \tag{3b}$$

$$\eta = \frac{R_L \omega^2 \chi^2}{(R_r+R_L)^2 \times \sum_{i=1}^{n-1} R_i I_i^2 + R_r \omega^2 \chi^2} \tag{3c}$$

where I_i is the current of transmitters, L_{ir} is the i^{th} trans coupling, R_L is the resistance of the load, R_i is the i^{th} transmitter series equivalent resistance, and R_r is the equivalent resistance of the receiver. As $k = \omega/R_L$ in (3b) is a constant, I_r has a direct relationship to the coordination factor χ. As such, the output power $P_{out} = R_L I_r^2$ has a direct relationship to χ^2. Therefore, hereinafter, current of receiver is selected to represent the output power. Furthermore, (3c) shows that the higher the χ, the higher the efficiency of the WPT coils. In this equation, $\sum_{i=1}^{n-1} R_i I_i^2$ represents the power losses in the transmitters, and it shows if the current in uncoupled coils is limited to zero, the efficiency will increase even more. This explains why different modes of operation is defined for the proposed system.

As the optimization of magnetic system is not the primary concern of this paper, transmitters and receivers are considered to be having identical dimensions with rectangular polarized structure. The parameters of coils are given in TABLE I. This arrangement of identical in-line transmitters is the simplest pattern that can be used and expandable either along the track or across its width. If transmitters are deployed in a regular manner, based on their pattern of deployment, some limited modes of operation can be defined to excite the transmitters and obtain the highest transferred power capacity with a minimum swing regardless of the number of transmitters.

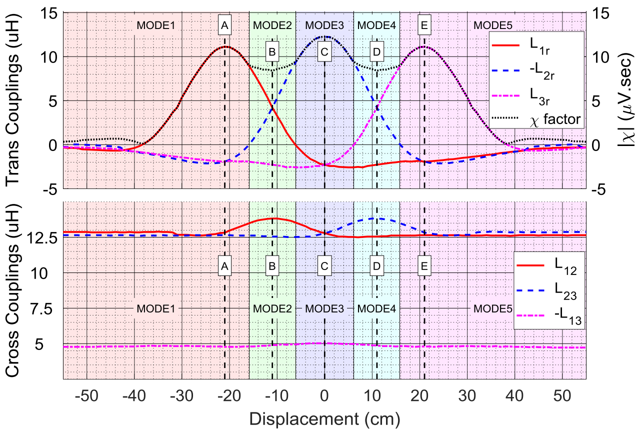

Fig. 5. Experimental results for trans couplings, coordination factor (χ) and cross coupling of a segmented DWPT system consisting of three transmitters and one receiver, based on the specifications of TABLE 1.

Fig. 5 shows the experimental magnetic profiles of a segmented DWPT system consisting of three transmitters (coils number one to three) and one receiver (r) obtained from the experimental measurements. Five main displacement positions (A, B, C, D, and E) are indicated in Fig. 5, where A, C, and E correspond to the aligned positions of transmitters 1, 2, and 3, respectively, and B and D are between transmitter pairs 1-2 and 2-3, respectively, where their mutual inductances are equal.

Here, with the use of the coordination factor, two basic modes of **single** and **overlap**, can be defined for the trans couplings. In single mode, only one transmitter interacts with the pickup, as shown in modes “1”, “3”, and “5” in Fig. 5, whereas in the overlap mode, two overlapped trans couplings, modes “2” and “4” in Fig. 5, with the pickup take place. For the given prototype, the pitch of transmitters is chosen so that there are two descending and incremental slopes for trans couplings for every overlapping adjacent coils seen by the receiver (r), as shown in overlap modes of “2” and “4”. A similar pattern can be replicated with the increase in the number of transmitters, as shown in Fig. 5.

As it is mentioned in section II, to keep the magnetic polarity of the identically wound windings in a segmented DWPT system the same, terminals of every other coil must be flipped when they are connected to the NLC output terminals. Using this, NLC can add up the effect of resultant fields in χ. Considering this fact for the obtained magnetic profile of the segmented DWPT in Fig. 5, five modes of operation can be defined. Taking mode “2” as an example, the sequence of signs for $[L_{1r}, -L_{2r}, L_{3r}]$ can be seen as [⊕,⊕,⊖]. Therefore, the effect of L_{1r} and L_{2r} can be added up by the converter with the selection of $[D_1, D_2, D_3, D_4]$ as $[0°, 180°, 0°, 0°]$ or $[180°, 0°, 180°, 180°]$ to obtain the highest possible χ in that region. Using the same analogy, different modes can be defined to obtain the highest possible χ at different pickup positions, as shown in Fig. 5. In the next section, using coupled inductors in the LCC compensator, the undesirable effect of cross coupling is addressed.

IV. COMPENSATION

Transmitter coils of the proposed segmented DWPT system is compensated with an integrated LCC compensator with coupled inductors [22], as shown in Fig. 6. LCC compensator at its resonant frequency acts as a current source and the variation of the reflected load from the pickup side does not influence the current amplitude in the transmitters. This feature makes the LCC to be a desirable choice for DWPT systems [12, 34-36]. Current in LCC primary loop ($I_{LS,i}$) can be defined as.

$$\begin{aligned}
I_{LS,i} = &\underbrace{\left(C_{P,i}L_{ii}\omega^2 - 1 - \frac{C_{P,i}}{C_{S,i}}\right) \times \left(j\overbrace{\omega C_{P,i} V_i}^{|I_i|}\right)}_{\substack{Quadrature\ term \\ (Independent)}} + \underbrace{\left(C_{P,i}\omega^2 \textstyle\sum_{k=1}^{n-2} L_{T,ii}\right) \times \left(j\overbrace{\omega C_{P,i} V_i}^{|I_i|}\right)}_{\substack{Quadrature\ term \\ (CPI\ self\ inductors)}} + \\
&\underbrace{C_{P,i}\omega^2 \sum_{\substack{k=1 \\ k\neq i}}^{n-1} L_{ki} \left(j\overbrace{\omega C_{P,k} V_k}^{|I_k|}\right)}_{\substack{Quadrature\ term \\ (Cross\ coupling)}} - \underbrace{C_{P,i}\omega^2 \sum_{\substack{k=1 \\ k\neq i}}^{n-1} L_{T,ki} \left(j\overbrace{\omega C_{P,k} V_k}^{|I_k|}\right)}_{\substack{Quadrature\ term \\ (CPI\ compensation)}} + \\
&\underbrace{\left(\frac{C_{P,i}}{Z_L} L_{iR}^2 \omega^3\right) \times \left(\overbrace{\omega C_{P,i} V_i}^{|I_i|}\right)}_{\substack{Direct\ term \\ (Reflected\ load)}} + \underbrace{\frac{C_{P,i}}{Z_L}\omega^3 \sum_{\substack{k=1 \\ k\neq i}}^{n-1} L_{ni} L_{kR} \left(\overbrace{\omega C_{P,k} V_k}^{|I_k|}\right)}_{\substack{Direct\ term \\ (Double\ reflected\ load)}}
\end{aligned} \tag{4}$$

where $C_{S,i}$, C_{Pi}, and L_{Si} are series capacitor, parallel capacitor, and series inductor of the LCC compensator respectively. L_{ij} and L_{ii} are the cross coupling and self-inductance of the transmitters, $L_{T,ij}$ and $L_{T,ii}$ are the cross coupling and self-inductance of the coupled inductors, Z_L is the compensated load at the pickup side, and V_i is the fundamental leg-to-leg voltage of the converter. The current of the transmitter I_i is given as $I_i = -j\omega C_{P,i} V_{i,1}$. Although, in the experimental prototype, cross couplings of all three transmitters are compensated using coupling inductors, for a realistic expanded system of $n-1$ coils for an NLC, the compensation of cross couplings due to at most two coils neighboring the excited coil would be sufficient. This is with reference to Fig. 5 depicting the cross couplings, where it shows that further the coil away from the excited coil, lower the effect of the cross couplings as L_{12} and L_{23} are significantly higher than L_{13}, and cross couplings would be negligible for more than two coils away from the excited coil.

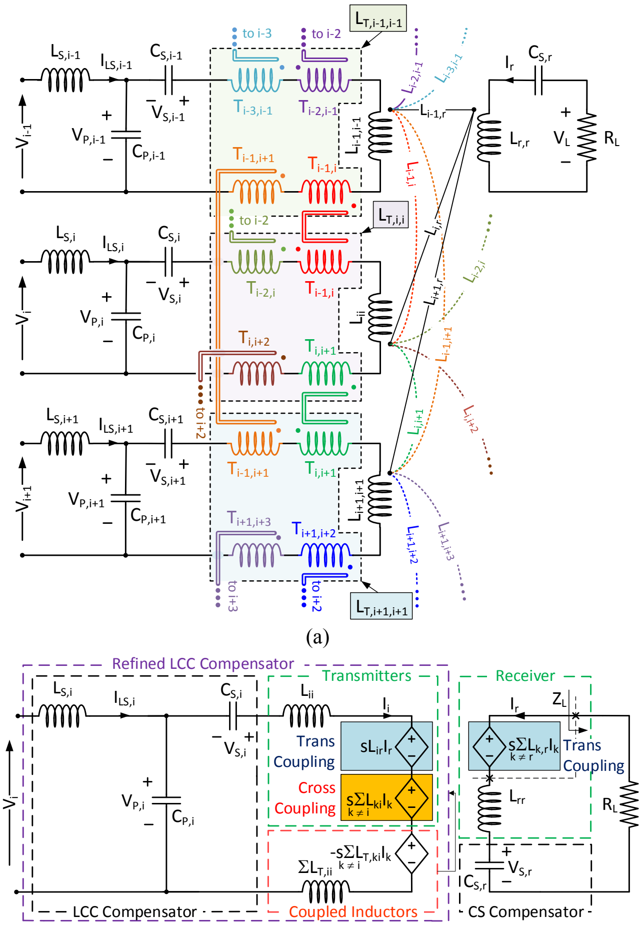

(a)

(b)

Fig 6. Circuit diagram showing an NLC supplying power through its refined LCC compensators to a series capacitor compensated pickup circuit. (a) Cross couplings and their compensation using three adjacent transmitters, $i-1$, i, and $i+1$ ($L_{T,ii}$ represents total self-inductances of coupled inductors in secondary loop of LCC. The coupled inductors are coupled by identical ferrites (double lines), and their specifications are given in TABLE 1), (b) Equivalent circuit for the i^{th} transmitter.

The simulation and theoretical waveforms of the transmitter current, I_i, and LCC primary loop current, $I_{LS,i}$, are shown in Fig. 7 and Fig. 8 respectively.

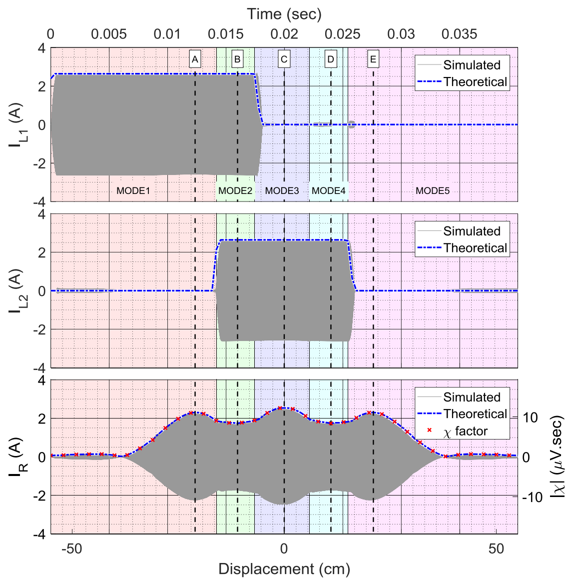

Fig. 7. Simulated and theoretical results for the currents of transmitters and receiver. The theoretical results are obtained from $I_i = -j\omega C_{P,i}V_{i,1}$ for the transmitter currents and (3b) for the receiver current.

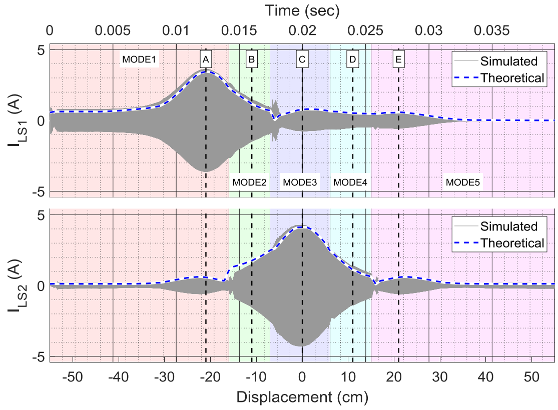

Fig. 8. Simulated and theoretical results for the LCC primary loop currents. The theoretical results are obtained from (4).

The theoretical results for $I_{LS,i}$ are obtained as the magnitude of the phasor expressions in (4), and the results for $I_{LEG,i}$ and I_i can be obtained in a similar way.

As shown in Fig. 5 and Fig. 7, as pickup gets closer to the transmitter number one, L_{1r} coupling starts to increase. Considering ⊕ and ⊖ for positive and negative values of trans couplings, respectively, in this mode, the trans couplings follow [⊕,⊖,⊖]. Therefore, exciting the converter with $[180^0, 0^0, 0^0, 0^0]$ will only energize the first coil, and pickup current will start to increase and follow the χ factor, as it is expected from (3b), as it reaches the second mode. In the second mode, the converter can excite the second transmitter to improve χ, as the trans coupling sequence of signs is [⊕,⊕,⊖], this can be done by applying $[0^0, 180^0, 0^0, 0^0]$ to NLC legs. When the converter enters the third mode of operation, the sequence of signs in trans couplings is [⊖,⊕,⊖]. Therefore, the use of $[0^0, 0^0, 180^0, 180^0]$ excitation will remove the undesirable effect of coils number one and three and maintain a higher level of transferred power in the system. The scenario can be replicated for n number of closely spaced transmitters located in a line. Although using a two-transmitter DWPT system would come up with the same result, for clarity, here, a three-transmitter DWPT system is used for demonstrations.

Considering x as the displacement axis of the pickup along the track, and $x = 0\,cm$ the center point of the middle transmitter, as shown in Fig. 1, the magnetic profile of the system is symmetric about $x = 0\,cm$, as shown in Fig. 5. Therefore, the current profile for the third transmitter is similar to the first transmitter mirrored along $x = 0\,cm$, the same is true for the LCC primary loop currents.

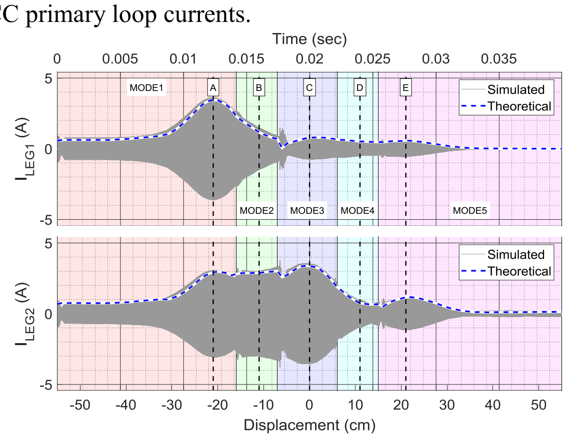

Fig. 9. Simulated and theoretical results for the LCC leg currents. The theoretical results are obtained by using (4) for the leg currents.

For clarity, the currents of the third transmitter and LCC primary loop is not shown in Figs. 7 and 8.

As for the leg currents, there are two types of legs in the system, lateral legs, i.e. leg 1 and leg n, and middle legs. Current in the lateral legs is $I_{Leg,1} = I_{LS,1}$ and $I_{Leg,n} = -I_{LS,n}$, and for the middle legs, it is $I_{LEG,i} = I_{LS,i} - I_{LS,i-1}$, where $1 < i < n$. Simulation and theoretical results for these currents are shown in Fig. 9 for legs 1 and 2. Legs 3 and 4 have the same pattern as legs 2 and 1 respectively, except that they are mirrored along $x = 0\ cm$. Therefore, they are not shown in the figure for clarity.

In (4), the quadrature components burden the power electronic switches with a severe hard switching, as they are 90 degrees out of phase with V_i and disrupt Zero Current Switching. To address this drawback, [37] suggests a method to tune C_{Si} to compensate the undesirable effects of self-inductances, and [22] uses coupled inductor to compensate the quadrature component of the induced voltage due to cross coupling.

The coupled inductors approach is used in this study, as shown in Fig. 6, in which they are tuned according to the following steps.

1. Find the cross couplings between the transmitters.
2. Design coupled inductors with a mutual inductance equal to the cross couplings, preferably with the same number of turns in primary and secondary sides.
3. Consider the effect of the primary and secondary self-inductances of coupled inductors in tuning the series capacitor of the LCC filter, based on [37].

To show how the refined LCC compensator helps the NLC with a desirable level of soft switching, simulation results shown in Fig. 10 compare converter leg currents feeding refined LCC compensator with that of unrefined LCC compensator at three different operational points of A, B, and C, which are shown in Figs. 5 to 9. The other operating points of D and E experience similar behavior as the system is symmetric about $x = 0\ cm$.

As shown in Fig. 10, the refined LCC compensator can make a desirable level of soft switching in the proposed system at different positions of the pickup.

V. Mode Changing Strategy

In the operation of the proposed NLC, occurrence of electric transients is unavoidable as operational modes keep changing according to the position of the pickup. Unlike mechanical dynamics, which are due to the pickup displacement, changes in the NLC modes of operation can happen in a fraction of a second and they produce a high level of electrical transients in the track-side driving systems. The harsh electrical transients usually lead to the failure of power electronic switches and malfunctioning of some coils. Therefore, such transients must be mitigated through an appropriate method. Here, a simple ramping pattern is proposed as a strategy to gradually change the mode of operation based on position feedback as shown in Fig 11 (a).

To find an appropriate ramping slope, the effect of dominant harmonics in the input voltage while it changes from one pattern to another is investigated.

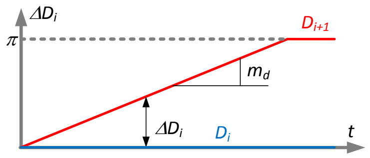

(a)

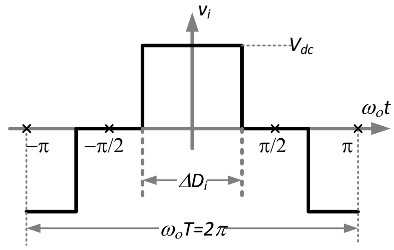

(b)

Fig. 11. Ramping strategy, (a) ramping of angles between two adjacent legs, and (b) generic NLC output voltage waveform.

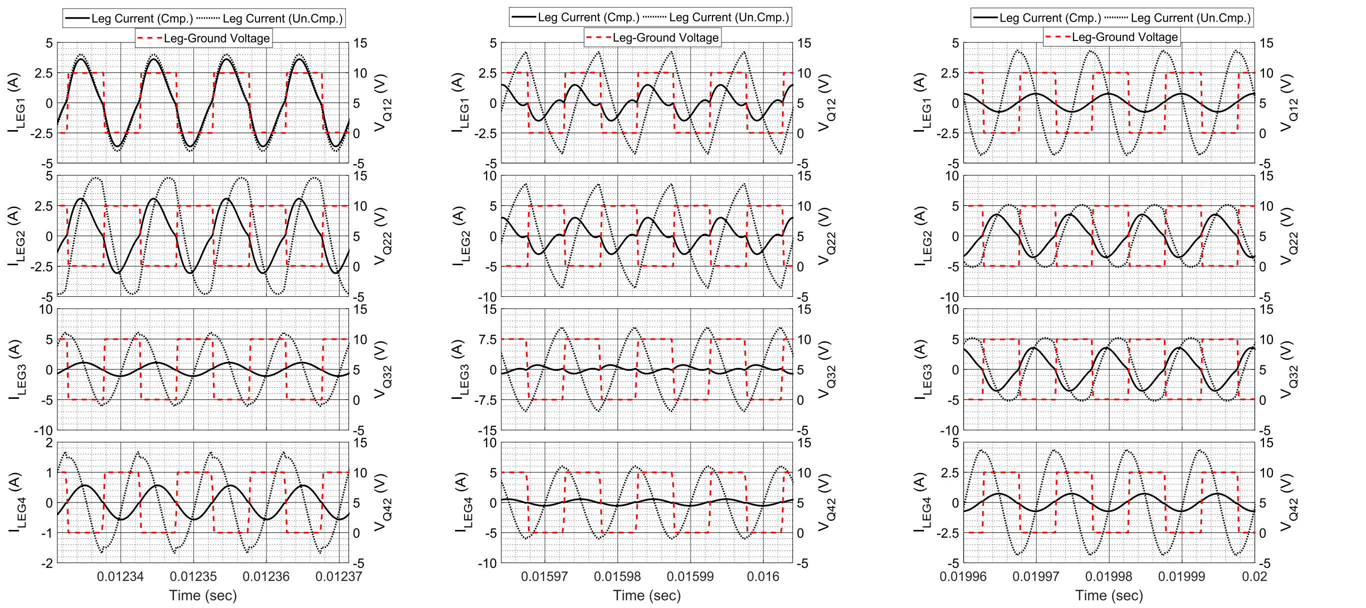

X(A) X(B) X(C)

Fig. 10. Simulated leg currents for the refined LCC compensated system in solid black line, and conventional LCC compensated system in dashed black line, which are compared with their corresponding leg-to-ground voltages for different positions of X(A), X(B), and X(C), shown in Fig. 5.

When the mode of operation changes, the phase angle between two adjacent legs varies. This can occur when either D_{i+1} or D_i changes. However, as $\Delta D_i = D_{i+1} - D_i = 180°$, simultaneous change in D_{i+1} and D_i results in a null voltage across the converter terminals when $D_{i+1}(t) = D_i(t)$ before they completely swap their angles.

Hence, to have a continuous flow of power during the transition, switching patterns are chosen so that only one leg changes its angle and get ramped. This change is not repetitive and cannot be described completely by Fourier based analysis, such as double Fourier method. Therefore, short-time Fourier transform (STFT) is used to describe the behavior of the applied waveform to the segmented DWPT transmitters in frequency domain [38]. For this purpose, it is considered that $\Delta D_i(t=0) = 0$ and it gradually increases to reach $\Delta D_i\left(t = \frac{\pi}{m_d}\right) = \pi$ with a rate of change of m_d, as shown in Fig. 11 (b).

This behavior can be represented by (5), and its time-varying Fourier component is $a_n(t)$ in (6). However, the variation of ΔD_i is a piecewise function, and according to (6), $x(t)$ can be described as (7), where $0 \le t < \frac{\pi}{m_d}$ is the window of STFT. After STFT calculations, the resulting frequency domain signal can be expressed as in (8).

$$\Delta D(t) = \begin{cases} m_d t; & 0 \le t < \dfrac{\pi}{m_d} \\ \pi; & \dfrac{\pi}{m_d} \le t \end{cases} \tag{5}$$

$$a_n(t) = \frac{2A}{\pi n} sin\left(\frac{\Delta D(t)}{2}\right) \tag{6}$$

$$x(t) = \begin{cases} \displaystyle\sum_{n=1}^{\infty} \frac{2A}{\pi n} sin\left(\frac{m_d t}{2}\right) cos(n\omega_0 t); & 0 \le t < \dfrac{\pi}{m_d} \\ \displaystyle\sum_{n=1}^{\infty} \frac{2A}{\pi n} cos(n\omega_0 t); & \dfrac{\pi}{m_d} \le t \end{cases} \tag{7}$$

$$X(\omega) = \frac{A}{\pi n} \times \sum_{n=1}^{\infty} \left(\begin{array}{c} \left[\frac{\left(\frac{m_d}{2}+n\omega_0\right)}{\left(\frac{m_d}{2}+n\omega_0\right)^2-\omega^2} + \frac{\left(\frac{m_d}{2}-n\omega_0\right)}{\left(\frac{m_d}{2}-n\omega_0\right)^2-\omega^2}\right] + \\ \left[\begin{array}{c} cos\left(n\omega_0\left(\frac{\pi}{m_d}\right)\right)\frac{j\omega}{(n\omega_0)^2-\omega^2} - \\ sin\left(n\omega_0\left(\frac{\pi}{m_d}\right)\right)\frac{n\omega_0}{(n\omega_0)^2-\omega^2} \end{array}\right] e^{-j\frac{\pi}{m_d}\omega} - \\ \left[\begin{array}{c} cos\left(\left(\frac{m_d}{2}+n\omega_0\right)\left(\frac{\pi}{m_d}\right)\right)\frac{\left(\frac{m_d}{2}+n\omega_0\right)}{\left(\frac{m_d}{2}+n\omega_0\right)^2-\omega^2} + \\ sin\left(\left(\frac{m_d}{2}+n\omega_0\right)\left(\frac{\pi}{m_d}\right)\right)\frac{j\omega}{\left(\frac{m_d}{2}+n\omega_0\right)^2-\omega^2} + \\ cos\left(\left(\frac{m_d}{2}-n\omega_0\right)\left(\frac{\pi}{m_d}\right)\right)\frac{\left(\frac{m_d}{2}-n\omega_0\right)}{\left(\frac{m_d}{2}-n\omega_0\right)^2-\omega^2} + \\ sin\left(\left(\frac{m_d}{2}-n\omega_0\right)\left(\frac{\pi}{m_d}\right)\right)\frac{j\omega}{\left(\frac{m_d}{2}-n\omega_0\right)^2-\omega^2} \end{array}\right] e^{-j\frac{\pi}{m_d}\omega} \end{array} \right) \tag{8}$$

As it is obvious from (8), the oscillating frequencies are $\omega_{sb,h} = \frac{m_d}{2} + n\omega_0$, $\omega_{bb} = n\omega_0$ and $\omega_{sb,l} = \frac{m_d}{2} - n\omega_0$, known as higher sideband harmonics, baseband harmonics, and lower sideband harmonics respectively. Following the same analogy, a similar result can be achieved for ramping with a negative slope.

These harmonics are responsible for triggering the oscillating natural frequencies of the system. On the other hand, bifurcation is an unavoidable phenomenon in weakly coupled WPT systems, such as the proposed system in this paper [15, 35]. This phenomenon bifurcates the natural oscillating frequency of the system into two. Consequently, bifurcation changes the natural response of the system. At bifurcated natural frequencies, the admittance seen from the NLC terminals is at its highest. Therefore, exciting the system near these frequencies results in a high flow of current and it can harm the components that are present in the current path, such as power electronic switches. Fig. 12. shows the admittance of the system from NLC terminals in logarithmic scale, when transmitters are fully coupled with the pickup (aligned) and when they are not coupled with the pickup (misaligned). In this figure, the baseband and sideband harmonics for three different slopes of ramping in ΔD_i, including $m_{d,1} = \frac{\omega_0}{20}$, $m_{d,2} = \frac{\omega_0}{100}$, and $m_{d,3} = \frac{\omega_0}{200}$, are shown. The higher and lower sideband harmonics are labelled respectively as f_h and f_l. According to Fig. 12 and (8), the lower the rate of change in ΔD_i, the closer the side band harmonics to the baseband harmonic, and the lower their effect on exciting bifurcated natural frequencies. This, however, may lead to increase in time for mode changing which is not desirable when pickup moves fast.

As it is noticed from Fig. 12, the strength of coupling can change the sensitivity of the system when the mode changes.

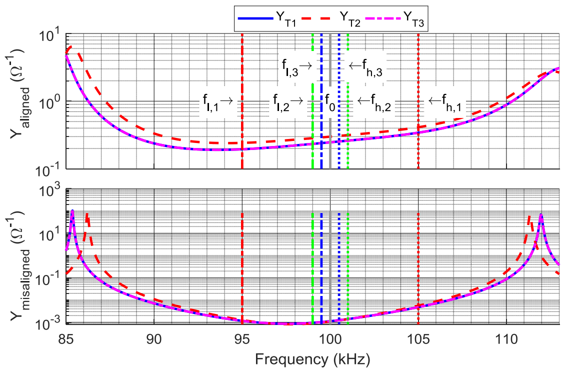

Fig. 12. Bifurcation phenomenon seen from the converter terminals at two effectively coupled (aligned) and weakly coupled (misaligned) positions. The dominant frequencies of the NLC output voltage waveform when it gradually ramps are shown in vertical lines for three different cases of m_{d1} $[f_{l,1}, f_{h,1}]$, m_{d2} $[f_{l,2}, f_{h,2}]$, and m_{d3} $[f_{l,3}, f_{h,3}]$.

In other words, the coil which is coupled weaker is more vulnerable to mode changing transients (admittance peaks of misaligned admittance in Fig. 23), and this can lead to failure in power electronic switches.

To see the effect of ramping at the given rates, the time domain transients in the first and second LCC primary loop currents and load current of the simulated system are shown in Fig. 13. This is carried out when the system mode of operation changes from “1” to “2”.

Therefore, according to trans coupling and admittance profiles, it is expected to see a more severe transients in the second primary loop current than the first one. Fig. 13 also shows that the decrease in the rate of ramping from a steep rate of m_{d1} to lower rates of m_{d2} and then m_{d3} can effectively suppress the mode changing transients. Therefore, compared to other complex methods, such as feedback controllers, ramping can be seen as a simple and effective strategy in mitigating mode changing transients.

In terms of reliability, the simplicity of this pattern is one of its outstanding features, especially when it is used in a converter with several power electronic switches, such as the proposed NLC, as opposed to a complex control strategy, which would significantly decrease the reliability of the overall system.

It is worthy to mention that unlike the steady modes of operation (modes “1”, “2”, “3”, and “4” in Figs 5 to 9), during the transition between two consecutive modes, ΔD_i can vary and take values between 0° to 180°. Fig. 14 shows the zoom-in transition window of Fig. 13 (a) for the first two legs and pickup currents, when the mode of operation changes from mode “1”, $[\Delta D_1, \Delta D_2, \Delta D_3] = [180°, 0°, 0°]$ to mode “2”, $[\Delta D_1, \Delta D_2, \Delta D_3] = [180°, 180°, 0°]$. As it can be seen in the period of transition, even though soft-switching cannot be fully met, with the refined LCC compensator during this period (solid black line), the converter performance is better than the unrefined compensator (dashed black line), as shown in Fig. 14.

Moreover, LCC compensators have a high quality factor and it can help the cancellation of side band harmonics and transients. Therefore, as shown in Fig. 14, transmitter transients will not affect the load current.

VI. Experimental Results:

To validate the abstract concepts of the proposed expandable NLC to drive closely spaced segmented DWPT systems, a laboratory prototype is built based on the specifications given in TABLE II, as shown in Fig.14. The experimental results are subsequently compared with the simulation results. The operation of the system when its pickup moves, soft switching at three different locations of A, B and C, shown in Fig. 5, and the effect of ramping strategy on suppressing the mode changing transients are the topics that are focused in experimental results.

As shown in Fig. 15, the experimental setup consists of three transmitters and one receiver. To study the operation of the system, the pickup is moved at a constant speed of 22 m/s. The NLC is supplied by a 10 V power supply which is filtered by a dc link capacitive bank having three parallel 2200 uF electrolyte capacitors. The segmented DWPT transmitters are compensated by the refined LCC compensators augmented by coupled inductors.

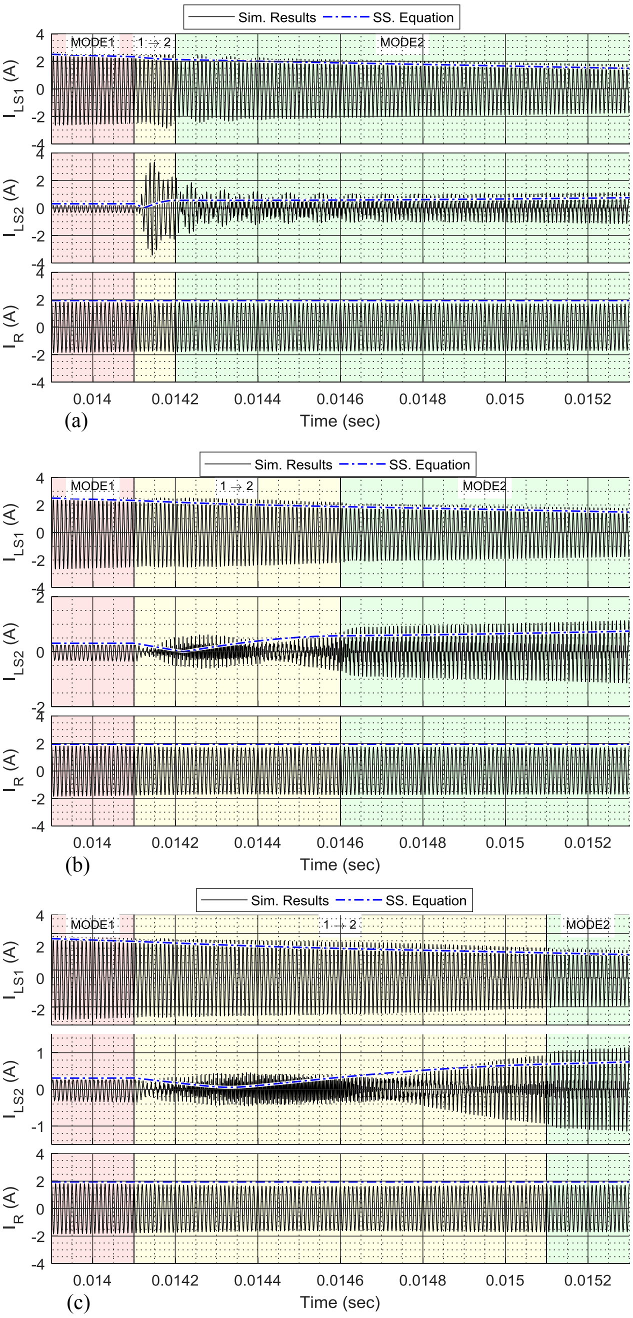

Fig. 13. Mode changing transients in the first and second LCC primary loop currents and the load current for three different cases of (a) m_{d1}, (b) m_{d2}, and (c) m_{d3}.

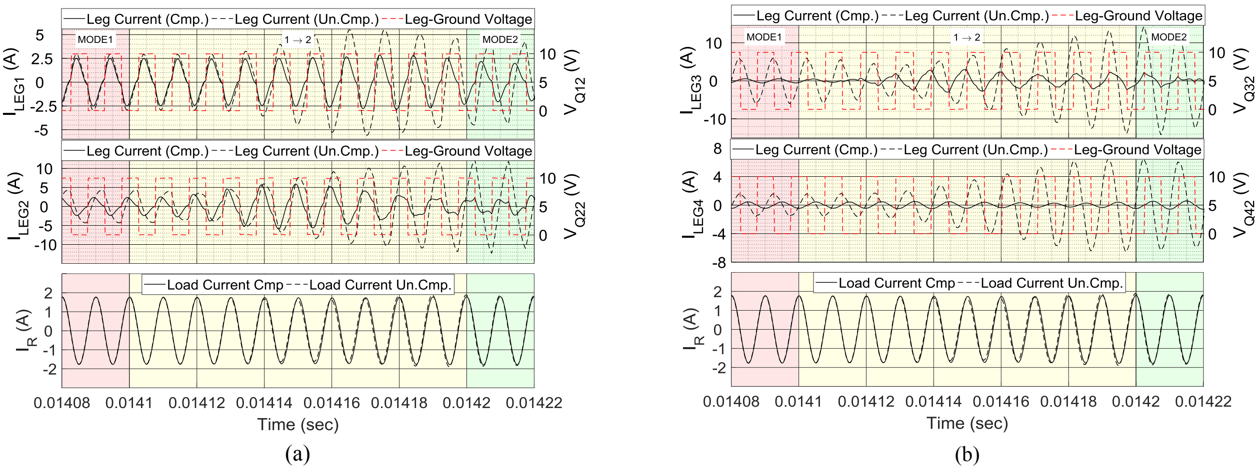

Fig. 14. Zoom-in of Fig. 13 (a) to see the effect of transitions between two modes (while $\Delta D_1 = 180°$ and ΔD_2 changes) on the (a) leg (“1” and “2”) and load currents, and (b) leg (“3” and “4”) with respect to the load current depicted in (a).

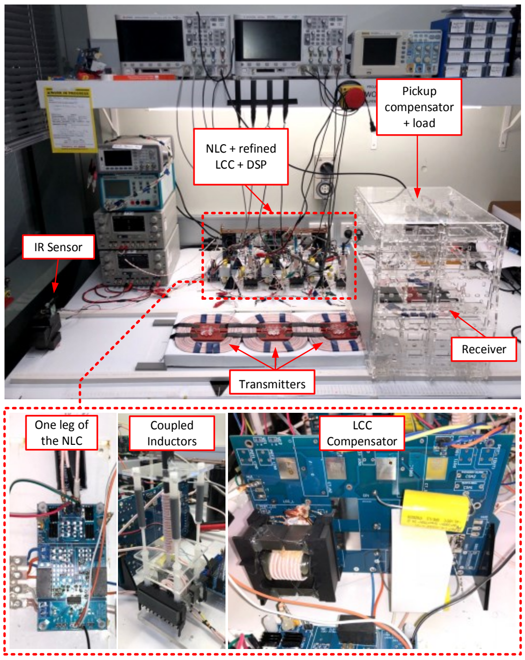

Fig. 15. Experimental setup of the NLC driving a closely spaced segmented DWPT system consisting of three transmitters and one receiver.

Based on the trans couplings, shown in Fig. 5, the modes of operation and their margins are defined for the controller to drive the NLC. The currents of the transmitters and receiver while the pickup moves are shown in Fig. 16. LCC primary loop currents are also shown in Fig. 17. From the experimental results, it can be clearly seen that the current profiles and their behavior are consistent with the simulation results. In addition, similar to Fig. 10, leg-to-ground voltage and leg current of each leg are measured for positions A, B, and C, and they are shown in Fig. 18. From the results, it can be seen that soft switching is completely achieved for steady modes of operation.

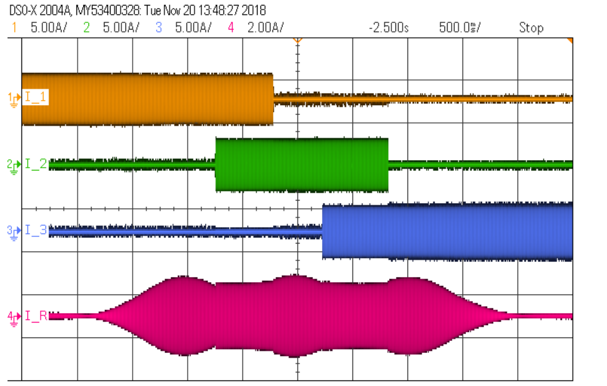

Fig. 16. Experimental results showing currents of the transmitters (I_1, I_2, and I_3) and receiver (I_r).

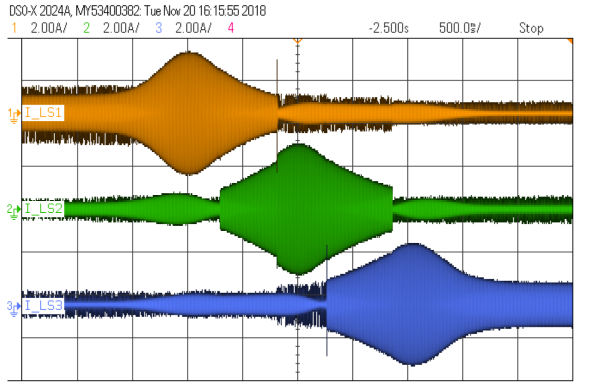

Fig. 17. Experimental results showing currents of the LCC primary loop for the transmitter compensators.

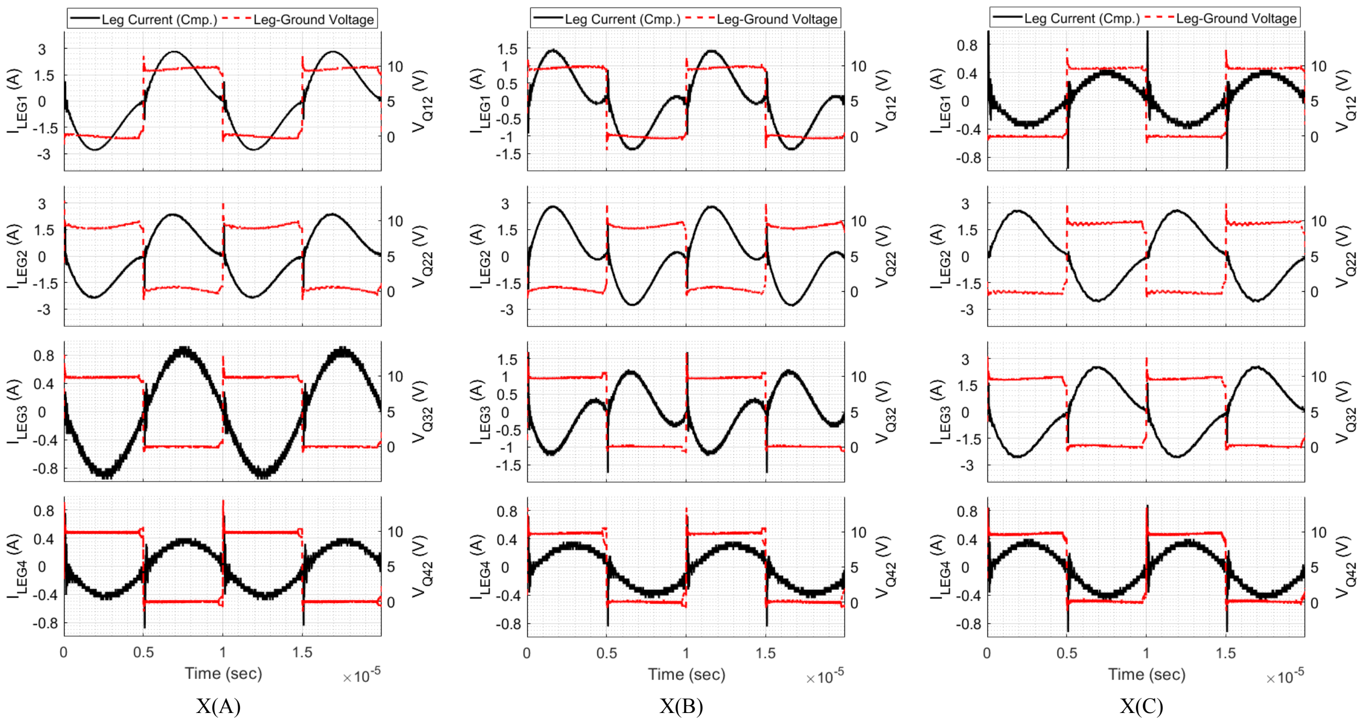

Fig. 18. Experimental results of the leg currents and leg-to-ground voltages at different positions of A, B, and C, shown in Fig. 5.

To further investigate the effect of coupling inductors on the soft switching, the efficiency of the NLC, and WPT coil-compensator are measured when the system is compensated by the coupling inductors and they are compared with the uncompensated case as shown in Fig. 19. The measurements are carried out for 23 different positions, and they clearly show that using coupling inductors, the efficiency of the NLC can be significantly improved. To represent the efficiency using a single number, an effective range of DWPT is considered from $x = -30\ cm$ to $30\ cm$, and the average of efficiencies are taken during this range. The obtained efficiencies for the NLC equipped with the coupling inductors, and without the coupling inductors are found to be 0.912 and 0.803 respectively, which shows 13.6 % of improvement in the converter efficiency with the use of coupling inductors.

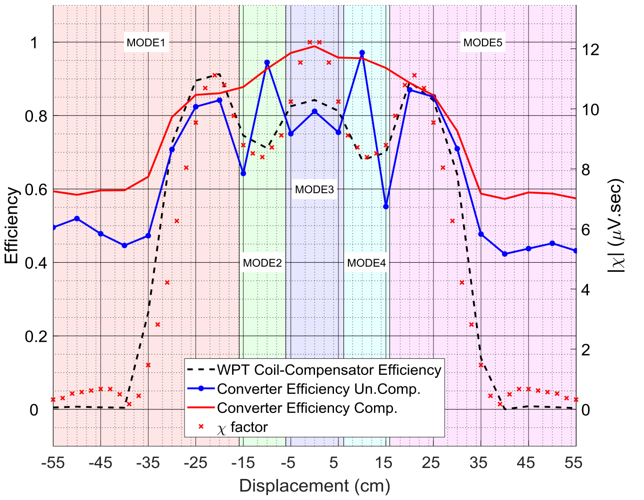

Fig. 19. Efficiency of the proposed converter when it is compensated by coupling inductors (red line), when each coil is independently compensated (starred blue line), and the efficiency of the WPT coil-compensator when the converter is compensated by the coupling inductors (dashed black line).

Fig. 19 shows the efficiency of coil-compensator in addition to the converter efficiency with and without coupling inductors. The figure also shows that there is a close relationship between the WPT coil-compensator efficiency and the coordination factor, which emphasizes the importance of the coordination factor, stated in (3d), to optimize the coil efficiency.

Moreover, the proposed mode changing algorithm is experimentally investigated for the ramping rates of $m_{d1} = 314.16\ krad/sec$, $m_{d2} = 69.813\ krad/sec$, and $m_{d3} = 39.270\ krad/sec$, when the mode of operation is changed from "1" to "2". The mode changing experimental results for the first and second LCC primary loop currents and load current are shown in Fig. 20, and they are consistent with the simulated results shown in Fig. 13. Moreover, to show how the transition influences the load and two first primary LCC loop currents, Fig. 21 shows a zoom-in view of Fig. 20 (a) during the transition, and the results are compatible with the simulation results.

As discussed before, quick ramping, such as m_{d2}, tends to trigger bifurcated natural frequencies and will result in high level of transients. Moreover, due to being closer to the mechanical transients, low rate of ramping, such as m_{d3}, is not desirable. Therefore, ramping rate is set to 69.813 $krad/s$ which is close to m_{d2}. Compared to mechanical transients, this rate of ramping is fast enough, and it can effectively suppress the mode changing transients. Therefore, the experimental results and simulation results show that the proposed methods are effective, reliable and economical for dynamic wireless charging systems.

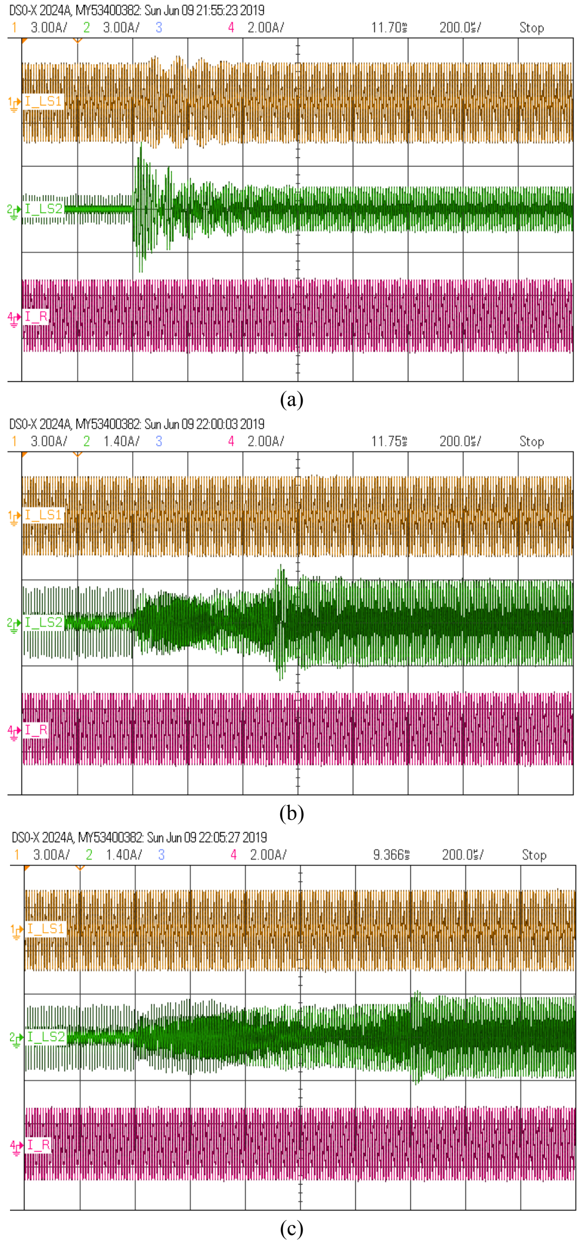

Fig. 20. Experimental results of mode changing transients in the first and second LCC primary loop currents and the load current for three different cases of (a) $m_{d1} = 314.16\ krad/sec$, (b) $m_{d2} = 69.813\ krad/sec$, and (c) $m_{d3} = 39.270\ krad/sec$.

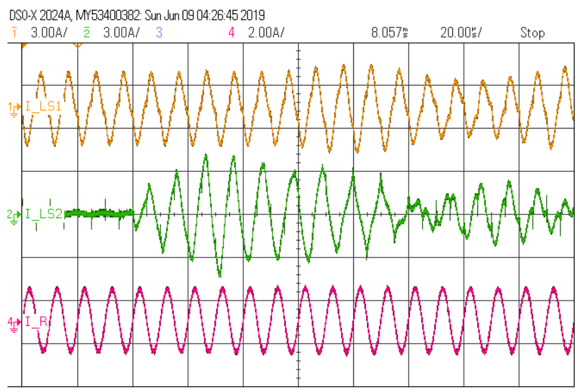

Fig. 21. Zoom-in view of transition in Fig. 20 (a).

APPENDIX

The specifications of the simulated and built system are given in TABLE. I. To have a better understanding about some geometric parameters, their dimensions are labelled in Fig. 22.

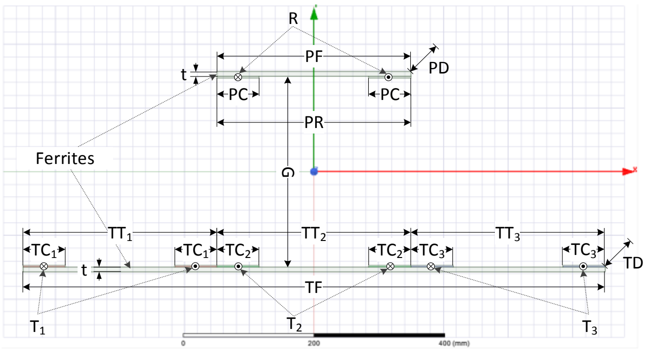

Fig. 22. 2D geometric representation of the segmented DWPT system.

TABLE I
Simulation and Experimental Specifications.

Parameters	Values
Track ferrite length (cm)	TF= 60.9
Track transmitter(s) length (cm)	[$TT_1 = TT_2 = TT_3$] = 20.3
Pickup receiver width (cm)	TD = 19.5
Track coil expansion (mm)	[$TC_1 = TC_3 = TC_2$] = 44
Track transmitter number of turns	[$N_{T1} = N_{T2} = N_{T3}$] = 16
Pickup ferrite length (cm)	PF = 20.3
Pickup receiver length (cm)	PR = 20.3
Pickup receiver width (cm)	PD = 22
Pickup coil expansion (mm)	PC = 31
Pickup receiver(s) number of turns	N_R = 11
Ferrite thickness (mm)	t = 7
Pickup - track gap distance (cm)	G = 12.5
Ferrite relative permeability	2300 (N97)
Maximum of track self-inductance (uH)	[$L_{11} = L_{33}, L_{22}$] = [92.2, 94.6]
Maximum of track cross couplings (uH)	[$L_{12} = L_{23}, L_{13}$] = [14, 5]
Maximum of pickup self-inductance (uH)	L_r = 53.9
WPT frequency (kHz)	f = 100
Track LCC series inductor (uH)	L_{si} = 7.67
Track LCC parallel capacitor (nF)	C_{pi} = 330
Track LCC series capacitor (nF)	C_{si} = [20.62]
Coupled inductors self-inductance (uH)	[$L_{T1} = L_{T3}, L_{T2}$] = [20, 17.6]
Coupled inductors mutual inductances (uH)	[$L_{12}^* = L_{23}^*, L_{13}^*$] = [14, 5]
Coupled inductors relative permeability	2200 (ETD49-N87)
Pickup series capacitor (nF)	C_{sr} = 47
Pickup coil resistance (Ohm)	R_{CP} = 0.076
Transmitter coil resistance (Ohm)	R_{CT} = 0.085
Load (Ohm)	R_L = 9

VII. CONCLUSION

In this paper, a new expandable converter known as N-legged Converter (NLC) is proposed to drive a multi transmitter wireless power transfer system for Dynamic WPT chargers. Owing to the controllability of transferred power flow in each transmitter, it can prevent the null of power and make a flatter and steadier transferred power profile at different pickup positions. The proposed technique can reduce the number of coils and the volume of ferrite in the pickup side, and as such gives enormous economic benefits as those components manufactured in mass. To make a uniform transferred power profile, the transmitters are positioned closely, and different modes of operation are defined for the NLC. As no currents flow through the non-interactive transmitters, there is a reduction in power losses. However, the proposed technique brings about the issues of cross coupling between transmitters and mode-changing transients. To address the undesirable effect of cross coupling on soft switching, a refined LCC compensator is proposed to maintain the soft switching regardless of the position of the pickup. In addition, a simple ramping strategy is used to suppress the mode changing transients. After analytically expressing the system, it is numerically simulated and experimentally tested, and the obtained results prove the credibility of the proposed techniques.

REFERENCES

[1] N. P. Suh and D. H. Cho, *The On-line Electric Vehicle: Wireless Electric Ground Transportation Systems*. Springer International Publishing, 2017.

[2] G. R. Nagendra, G. A. Covic, and J. T. Boys, "Sizing of Inductive Power Pads for Dynamic Charging of EVs on IPT Highways," *IEEE Transactions on Transportation Electrification,* vol. 3, no. 2, pp. 405-417, 2017, doi: 10.1109/TTE.2017.2666554.

[3] A. Y. S. Lam, Y. Leung, and X. Chu, "Electric Vehicle Charging Station Placement: Formulation, Complexity, and Solutions," *IEEE Transactions on Smart Grid,* vol. 5, no. 6, pp. 2846-2856, 2014, doi: 10.1109/TSG.2014.2344684.

[4] S. Li and C. C. Mi, "Wireless Power Transfer for Electric Vehicle Applications," *IEEE Journal of Emerging and Selected Topics in Power Electronics,* vol. 3, no. 1, pp. 4-17, 2015, doi: 10.1109/JESTPE.2014.2319453.

[5] C. T. Rim and C. Mi, *Wireless Power Transfer for Electric Vehicles and Mobile Devices*. Wiley, 2017.

[6] M. Budhia, J. T. Boys, G. A. Covic, and C. Y. Huang, "Development of a Single-Sided Flux Magnetic Coupler for Electric Vehicle IPT Charging Systems," *IEEE Transactions on Industrial Electronics,* vol. 60, no. 1, pp. 318-328, 2013, doi: 10.1109/TIE.2011.2179274.

[7] F. Musavi and W. Eberle, "Overview of wireless power transfer technologies for electric vehicle battery charging," *IET Power Electronics,* vol. 7, no. 1, pp. 60-66, 2014, doi: 10.1049/iet-pel.2013.0047.

[8] A. Khaligh and S. Dusmez, "Comprehensive Topological Analysis of Conductive and Inductive Charging Solutions for Plug-In Electric Vehicles," *IEEE Transactions on Vehicular Technology,* vol. 61, no. 8, pp. 3475-3489, 2012, doi: 10.1109/TVT.2012.2213104.

[9] M. Yilmaz, V. T. Buyukdegirmenci, and P. T. Krein, "General design requirements and analysis of roadbed inductive power transfer system for dynamic electric vehicle charging," in *2012 IEEE Transportation Electrification Conference and Expo (ITEC)*, 18-20 June 2012 2012, pp. 1-6, doi: 10.1109/ITEC.2012.6243497.

[10] S. Choi, J. Huh, W. Y. Lee, S. W. Lee, and C. T. Rim, "New Cross-Segmented Power Supply Rails for Roadway-Powered Electric Vehicles," *IEEE Transactions on Power Electronics,* vol. 28, no. 12, pp. 5832-5841, 2013, doi: 10.1109/TPEL.2013.2247634.

[11] K. Lee, Z. Pantic, and S. M. Lukic, "Reflexive Field Containment in Dynamic Inductive Power Transfer Systems," *IEEE Transactions on Power Electronics,* vol. 29, no. 9, pp. 4592-4602, 2014, doi: 10.1109/TPEL.2013.2287262.

[12] S. Zhou and C. C. Mi, "Multi-Paralleled LCC Reactive Power Compensation Networks and Their Tuning Method for Electric Vehicle Dynamic Wireless Charging," *IEEE Transactions on Industrial Electronics,* vol. 63, no. 10, pp. 6546-6556, 2016, doi: 10.1109/TIE.2015.2512236.

[13] Y. Guo, L. Wang, Q. Zhu, C. Liao, and F. Li, "Switch-On Modeling and Analysis of Dynamic Wireless Charging System Used for Electric Vehicles," *IEEE Transactions on Industrial Electronics,* vol. 63, no. 10, pp. 6568-6579, 2016, doi: 10.1109/TIE.2016.2557302.

[14] J. Huh, S. W. Lee, W. Y. Lee, G. H. Cho, and C. T. Rim, "Narrow-Width Inductive Power Transfer System for Online Electrical Vehicles," *IEEE Transactions on Power Electronics,* vol. 26, no. 12, pp. 3666-3679, 2011, doi: 10.1109/TPEL.2011.2160972.

[15] W. Chwei-Sen, G. A. Covic, and O. H. Stielau, "Power transfer capability and bifurcation phenomena of loosely coupled inductive power transfer systems," *IEEE Transactions on Industrial Electronics,* vol. 51, no. 1, pp. 148-157, 2004, doi: 10.1109/TIE.2003.822038.

[16] J. P. K. Sampath, D. M. Vilathgamuwa, and A. Alphones, "Efficiency Enhancement for Dynamic Wireless Power Transfer System With Segmented Transmitter Array," *IEEE Transactions on Transportation Electrification,* vol. 2, no. 1, pp. 76-85, 2016, doi: 10.1109/TTE.2015.2508721.

[17] J. M. Miller *et al.*, "Demonstrating Dynamic Wireless Charging of an Electric Vehicle: The Benefit of Electrochemical Capacitor Smoothing," *IEEE Power Electronics Magazine,* vol. 1, no. 1, pp. 12-24, 2014, doi: 10.1109/MPEL.2014.2300978.

[18] O. C. Onar, J. M. Miller, S. L. Campbell, C. Coomer, C. P. White, and L. E. Seiber, "A novel wireless power transfer for in-motion EV/PHEV charging," in *2013 Twenty-Eighth Annual IEEE Applied Power Electronics Conference and Exposition (APEC)*, 17-21 March 2013 2013, pp. 3073-3080, doi: 10.1109/APEC.2013.6520738.

[19] F. Lu, H. Zhang, H. Hofmann, and C. C. Mi, "A Dynamic Charging System With Reduced Output Power Pulsation for Electric Vehicles," *IEEE Transactions on Industrial Electronics,* vol. 63, no. 10, pp. 6580-6590, 2016, doi: 10.1109/TIE.2016.2563380.

[20] A. Zaheer, H. Hao, G. A. Covic, and D. Kacprzak, "Investigation of Multiple Decoupled Coil Primary Pad Topologies in Lumped IPT Systems for Interoperable Electric Vehicle Charging," *IEEE Transactions on Power Electronics,* vol. 30, no. 4, pp. 1937-1955, 2015, doi: 10.1109/TPEL.2014.2329693.

[21] Y. Tian, J. Tian, D. Li, and S. Zhou, "A Multiple Legs Inverter with Real Time–Reflected Load Detection Used in the Dynamic Wireless Charging System of Electric Vehicles," *Energies,* vol. 11, no. 5, p. 1275, 2018. [Online]. Available: https://www.mdpi.com/1996-1073/11/5/1275.

[22] F. Farajizadeh, M. Vilathgamuwa, P. Jayathurathnage, G. Ledwich, and U. K. Madawala, "Soft Switching in Closely Spaced Multi-Transmitter Wireless Power Transfer Systems," in *45 Annual Conference of the Industrial Electronics*, Lisbon, Portugal, 14-17 Oct. 2019.

[23] F. Farajizadeh, M. Vilathgamuwa, P. Jayathurathnage, and G. Ledwich, "Expandable N-Legged Converter for Dynamic Wireless Power Transfer," in *2018 IEEE 18th International Power Electronics and Motion Control Conference (PEMC)*, 26-30 Aug. 2018, pp. 115-120, doi: 10.1109/EPEPEMC.2018.8521754.

[24] A. Lusiewicz, J. Noeren, M. Jaksch, and N. Parspour, "A Novel Method for Online Coupling Factor Determination in Inductive Power Transfer Systems," in *2018 IEEE Wireless Power Transfer Conference (WPTC)*, 3-7 June 2018 2018, pp. 1-4, doi: 10.1109/WPT.2018.8639460.

[25] S. Li and S. Y. R. Hui, "Comparative Study on Front-End Parameter Identification Methods for Wireless Power Transfer Without Wireless Communication Systems," in *2018 International Power Electronics Conference (IPEC-Niigata 2018 -ECCE Asia)*, 20-24 May 2018 2018, pp. 2552-2557, doi: 10.23919/IPEC.2018.8507669.

[26] M. Khalilian, S. G. Rosu, V. Cirimele, P. Guglielmi, and R. Ruffo, "Load identification in dynamic wireless power transfer system utilizing current injection in the transmitting coil," in *2016 IEEE Wireless Power Transfer Conference (WPTC)*, 5-6 May 2016 2016, pp. 1-4, doi: 10.1109/WPT.2016.7498793.

[27] Y. Shin, K. Hwang, J. Park, D. Kim, and S. Ahn, "Precise Vehicle Location Detection Method Using a Wireless Power Transfer (WPT) System," *IEEE Transactions on Vehicular Technology,* vol. 68, no. 2, pp. 1167-1177, 2019, doi: 10.1109/TVT.2018.2885942.

[28] W. Han, K. T. Chau, C. Jiang, and W. Liu, "Accurate Position Detection in Wireless Power Transfer Using Magnetoresistive Sensors for Implant Applications," *IEEE Transactions on Magnetics,* vol. 54, no. 11, pp. 1-5, 2018, doi: 10.1109/TMAG.2018.2843796.

[29] K. Hwang, J. Cho, J. Park, D. Har, and S. Ahn, "Ferrite Position Identification System Operating With Wireless Power Transfer for Intelligent Train Position Detection," *IEEE Transactions on Intelligent Transportation Systems,* vol. 20, no. 1, pp. 374-382, 2019, doi: 10.1109/TITS.2018.2797991.

[30] *ANSYS Electronics\Maxwell*. (2016). [Online]. Available: https://ansyshelp.ansys.com/account/secured?returnurl=/Views/Secured/Electronics/v180/home.htm%23

[31] *MATLAB*. (2017).

[32] R. Johari, J. V. Krogmeier, and D. J. Love, "Analysis and Practical Considerations in Implementing Multiple Transmitters for Wireless Power Transfer via Coupled Magnetic Resonance," *IEEE Transactions on Industrial Electronics,* vol. 61, no. 4, pp. 1774-1783, 2014, doi: 10.1109/TIE.2013.2263780.

[33] F. Kong, "Coil misalignment compensation techniques for wireless power transfer links in biomedical implants," 10016427 M.S., Rutgers The State University of New Jersey - New Brunswick, Ann Arbor, 2015.

[34] J. Hou, Q. Chen, Z. Zhang, S. C. Wong, and C. K. Tse, "Analysis of Output Current Characteristics for Higher Order Primary Compensation in Inductive Power Transfer Systems," *IEEE Transactions on Power Electronics,* vol. PP, no. 99, pp. 1-1, 2017, doi: 10.1109/TPEL.2017.2755862.

[35] W. Zhang and C. C. Mi, "Compensation Topologies of High-Power Wireless Power Transfer Systems," *IEEE Transactions on Vehicular Technology,* vol. 65, no. 6, pp. 4768-4778, 2016, doi: 10.1109/TVT.2015.2454292.

[36] Jurgen Meins, Gunther Buhler, Robert Czainski, and F. Turki, "Contactless inductive power supply," presented at the Proc. 19th Int. Conf. Magn. Levitated Syst. Linear Drives, Sep. 2006.

[37] Z. Pantic, S. Bai, and S. M. Lukic, "ZCS LCC-Compensated Resonant Inverter for Inductive-Power-Transfer Application," *IEEE Transactions on Industrial Electronics,* vol. 58, no. 8, pp. 3500-3510, 2011, doi: 10.1109/TIE.2010.2081954.

[38] K. Gröchenig, "The Short-Time Fourier Transform," in *Foundations of Time-Frequency Analysis*. Boston, MA: Birkhäuser Boston, 2001, pp. 37-58.